IEEE Photonics Journal
An IEEE Photonics Society Publication

Open Access

Size-Dependent Multiple-Scattering Effects of Mesoporous TiO_2 Beads Distinguished by Optical Coherence Tomography

Volume 9, Number 5, October 2017

Ling-Hsuan Tsai
Po Nien Yang
Yen-Chen Shih
King-Fu Lin
Chung-Chih Wu
Hoang Yang Lin

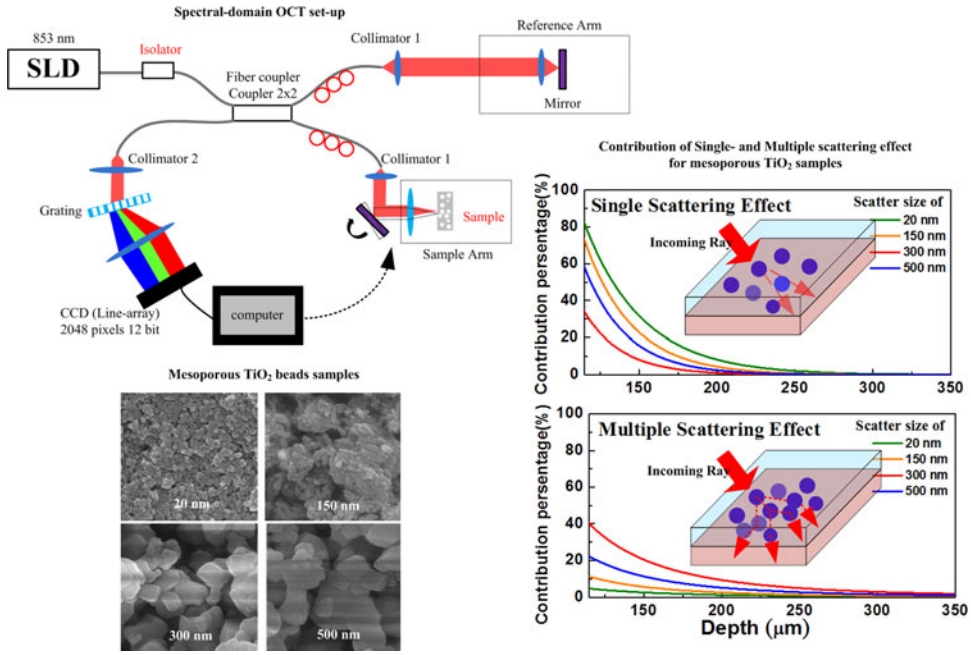

DOI: 10.1109/JPHOT.2017.2734566
1943-0655

Size-Dependent Multiple-Scattering Effects of Mesoporous TiO_2 Beads Distinguished by Optical Coherence Tomography

Ling-Hsuan Tsai,[1] Po Nien Yang,[1] Yen-Chen Shih,[2] King-Fu Lin,[2] Chung-Chih Wu,[1] and Hoang Yang Lin[1]

[1]Graduate Institute of Photonics and Optoelectronics, and Department of Electrical Engineering, National Taiwan University, Taipei 10617, Taiwan
[2]Department of Materials Science and Engineering, National Taiwan University, Taipei 10617, Taiwan

DOI:10.1109/JPHOT.2017.2734566

Manuscript received June 15, 2017; revised July 21, 2017; accepted July 25, 2017. Date of publication July 31, 2017; date of current version October 5, 2017. This work was supported in part by the Ministry of Science and Technology of Taiwan under Contract MOST 106-2221-E-002-155-MY3, Contract 105-2221-E-002-121, and Contract MOST 106-3113-E-155-001-CC2 and in part by the National Taiwan University under the Aim for Top University Project 105R8908. Corresponding author: Hoang Yang Lin (e-mail: hylin@cc.ee.ntu.edu.tw).

Abstract: In this study, we propose a new analysis method using optical coherence tomography to further use the diffusive reflectance measurement to quantify the contribution of the size-dependent multiple-scattering effects of mesoporous TiO_2 beads. The diffusive reflectance results from the complex interactions between light and the scattering particles, and influences the slopes of the associated depth-dependent A-scan profiles, which can be fitted based on the extended Huygens–Fresnel model to quantify the contribution ratio of the multiple-scattering effects to the single scattering effects. The mesoporous TiO_2 beads with average diameter of 300 nm show higher contribution percentage of multiple-scattering effects inducing reflectivity enhancement in the longer wavelength region. The contribution ratio of multiple-scattering effects can be distinguished numerically, and is enhanced from 5% to 40% and then decreased to 20% for the bead diameters ranging from 20 to 300 nm and then to 500 nm, respectively. The calculated scattering coefficients are $13.5 \pm 0.6\ mm^{-1}$, $16.5 \pm 0.6\ mm^{-1}$, $20.2 \pm 0.6\ mm^{-1}$, and $18.5 \pm 0.6\ mm^{-1}$, respectively.

Index Terms: Optical coherence tomography, multiple scattering, light scattering interaction.

1. Introduction

In various optoelectronics applications, crystalline mesoporous titanium dioxide (TiO_2) beads are widely used for their scattering properties [1]–[3]. Especially in DSSC devices, macroporous TiO_2 spheres of various sizes were commonly utilized in the light scattering layer to improve the device efficiency [4]. Also, having TiO_2 particles (15–40 nm particle size) in the transparent layer can improve the absorption efficiency of the dye, and larger TiO_2 particles can be used in the scattering layer to improve the light harvesting, and enhance the effective photocurrent generation [5], [6]. Generally, a common method to measure the scattering is to measure the far-field scattering distribution directly, usually represented as a function of the light intensity [7]. However, this is

difficult with inhomogeneous materials, especially for samples with irregular shapes and structures [6], [8].

For single particle scattering, the scattered field (based on the Mie scattering model) is relatively well documented [9]–[11]. However, the actual scattering layer in an optoelectronic device is rarely as simple as a single scattering particle embedded in the medium. The scattering of light is a complex interaction between multiple photons and scattering particles, such that the complete description of the scattering has components from single scattering and multiple scattering [12]. Furthermore, the contribution of both single and multiple scattering effects are strongly influenced by different properties of the scattering sample such as the sizes, structures, and concentration of the scattering particle, and the inter-particle spacing (IPS). In particular, French *et al.* reported that multiple scattering effects occurs within different concentrations of TiO_2 scattering particles embedded in transparent turbid medium, and the diffusive reflectance showed that the enhancement of reflectivity at the longer wavelength region is a result of the multiple scattering effects, and is theoretically simulated by numerical methods [13], [14]. In [14], Mcneil *et al.* reported the simulated multiple scattering function against scattering angle based on Kubelka-Munk two-stream formulation. However, there is a limitation in this calculation process for the longer wavelength region, and the Kubelka-Munk parameters can be unavailable without absorption effect.

The advantages of OCT are non-contact, non-destructive, and high-resolution analysis technique, first reported by Fujimoto in 1991 [15], and has seen much developments in recent years. In OCT systems, light from the backscattering of the sample interferes with the reference light, to provide the signal as a function of depth, which carries the unique optical information of examined samples, specifically, the scattering coefficient (μ_s) and the anisotropy factor (g). For the past few years, the OCT technique is not only applied to the medical field, but also used for the analysis of optical devices and semiconductor materials ex-vivo [16]–[18]. In addition, the optical properties of nanoparticle used as the contrasting agent in the cell tissues to enhance the image quality had also been analyzed using OCT system [19], [20]. In this study, we utilize the SD-OCT system to analyze the scattering occurring in mesoporous TiO_2 samples with different bead diameters and morphologies. Combining with signal processing algorithms, the interferometer signals can be extracted as functions of depths (A-scan profiles). Furthermore, the scattering angle and scattering coefficient can be fitted with the extended Huygens-Fresnel (EHF) model [21].

In addition, these two papers [22], [23] have demonstrated the interferometer signals of OCT system and these signals can be described based on EHF theory or Monte Carlo simulation with further consideration of multiple scattering effects. Despite Monte Carlo method is an alternative method to simulate the OCT signal in depth, the EHF theory is more comprehensive to quickly calculate and easier to optimize the system parameters [24]. In our study, we also adopted the EHF theory to execute the fitting process of mesoporous TiO_2 bead samples for obtaining the essential optical properties. Different from [22], we further calculate the IPS of mesoporous TiO_2 beads with different diameters and try to discuss the relationship between IPS and the contribution percentages of single and multiple scattering effects. Finally, the single and multiple scattering effects can be distinguished, and correlated to the density of the scattering particles to provide optimal results for utilizing mesoporous TiO_2 beads in various optoelectronic applications.

2. Experimental Details

2.1 Preparation of Mesoporous TiO_2 Beads

The mesoporous TiO_2 beads of 20–500 nm diameter were coated on glass substrates by the sol-gel process. The fixed weight fraction was prepared as 13 wt% of TiO_2 powders (US Research Nanomaterials, Inc) by using isopropyl alcohol (IPA) and DI water. The TiO_2 pastes were obtained by adding poly ethylene glycol (PEG) to a TiO_2 solution of 30% concentration, after stirring for a length of time exceeding one week. Then, using the adhesive tape as a spacer ($\sim$120 μm thickness), the TiO_2 pastes were spread onto the substrate using a glass rod. The TiO_2 pastes prepared on the glass substrates were heated in an oven at 450 °C for 30 minutes to remove the solvent solution.

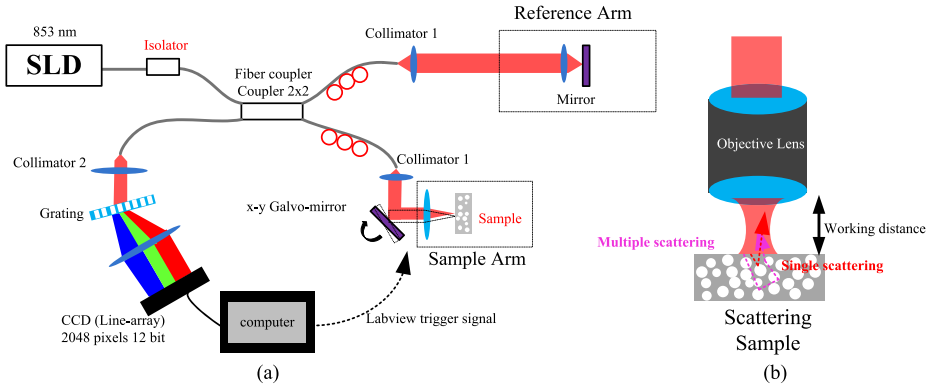

Fig. 1. (a) Schematic diagram of SD-OCT system with SLD source at the central wavelength of 850 nm, and the mesoporous TiO_2 beads are placed on the sample arm. (b) Magnified schematic diagram of the sample arm and scattering effects of a mesoporous TiO_2 film are shown.

The result is a mesoporous TiO_2 thin film with different bead diameters, composed of TiO_2 beads and air, on the glass substrates. In general, the samples with homogeneous scatters are usually assumed and employed for most applications. Although the scatters are assumed as homogeneous in the film, they are randomly distributed and can be quantified by the volume fraction defined below.

2.2 Experiment and Characterization

The schematic of the SD-OCT system is shown in Fig. 1(a). A super-luminescent diode (SLD) as a low temporal coherence light source is used in this system, with the wavelength centered at 853 nm and 30 nm FWHM. The measured resolution, by setting a mirror at the sample arm, is 13 μm in air. A single mode fiber (Thorlabs 780HP) directs light from the source into a 2 $\times$ 2 50:50 fiber coupler, into the reference and sample arms. At the sample arm, the objective lens (Thorlabs LSM02-BB) has effective focal length (f) of 17.93 mm, and samples of TiO_2 beads with different diameters have been measured at a working distance of 7.5 mm, and the numerical aperture (NA) is 0.042. Before acquiring the interferometer signal, the best measurement position will be found by adjusting the samples to approach the sharp focus to obtain the highest power back-reflected from samples. In general, this measurement position can be indicated at the working distance which is defined as the distance between the front surface of objective lens and the closest surface of sample. The backscattered light collected from the sample interferes with the reflection from the reference arm, and the interference signal was directed to a transmission grating (1200 lines/mm) and focused onto the CCD (e2V, 2048 pixels), with line rate of 28 kHz.

The OCT signals of TiO_2 bead samples with different diameters have been averaged over 1000 measurements (A-scan profiles) at the same location without moving the galvo mirror, and subtracted by the reference arm intensity to obtain the interferometer signal without the DC term. The signal is processed to obtain the interference spectrum, which in turn is analyzed to obtain the scattering properties of the measured sample. In addition, the diffusive reflectance spectra of the mesoporous TiO_2 beads of various average diameters are measured by a spectrophotometer (Perkine-Elmer Lamda 35) in the wavelength range of 300$\sim$1100 nm with an integrating sphere (Perkin-Elmer Labshphere RSA-PE-20). The field emission scanning electron microscope (SEM, JEOL JSM-6700F) was used to confirm the morphology of the mesoporous TiO_2 scatter films prepared on the glass substrates. The thickness of the mesoporous TiO_2 films was obtained by an alpha-step instrument (Kosaka Laboratory Ltd. ET3000).

2.3 Theoretical Curve Fitting by the Extended Huygens-Fresnel Model

Here, the optical properties of the mesoporous TiO_2 beads are determined using the extended Huygens-Fresnel (EHF) theory, which is based on the beam propagation in the geometric structure

of sample arm [21]. By using this model, we are able to take into account both the single and multiple scattering effects of mesoporous TiO_2 beads, whereas the Mie scattering model considers only the single scattering of a spherical scattering particle. Furthermore, the A-scan signal of the OCT can be represented as a function of the scattering coefficient (μ_s) and scattering angle (θ_{rms}). As shown in (1), the heterodyne signal current $<i^2(z)>$ as a function of depth z is used to represent the A-scan signal profile detected in the OCT system and can be expressed as the product of the parameter N and heterodyne factor $\psi(z)$. Here, N is a fixed constant related to the parameters used in this OCT system and $\psi(z)$ is a heterodyne factor which will be varied depending on the different optical properties for each TiO_2 bead sample. According to the [21], (1) can be derived from the physical phenomenon of light propagating through the tissue with mutual coherence function. The heterodyne factor $\psi(z)$ in (1) can be decomposed into three terms as in (2), the first and third terms are principally the contributions of single- and multiple- scattering effects, which can be expressed as the functions of depth by fixing the scattering coefficient. In addition, the second term is the cross term for coherent mixing of the unscattered and multiple-scattering light [25]. Therefore, we consider only the first and third terms for the pure contribution of single- and multiple-scattering light. The parameters P_R and P_S are the powers at the reference and sample arms, α is the quantum conversion efficiency of CCD, σ_b is backscattering cross-section, and w_H and w_S are the 1/e irradiance radii in the absence and presence of scattering, respectively. The parameter $\psi(z)$ is a heterodyne factor, which has a strongly correlation with the scattering coefficient μ_s of the mesoporous TiO_2 beads, and is attributed to the single and multiple scattering effects. The proportion of w_H and w_S can also be written in the form of (2), where the ρ_0 is the lateral coherence length, correlated with the scattering angle θ_{rms}, the refractive index n, the beam waist w_0 of sample beam, and the focal length f of objective lens.

$$<i^2(z)> = N\psi(z) \tag{1}$$

$$\psi(z) = \left[\exp(-2\mu_s z) + \frac{2\exp(-\mu_s z)[1-\exp(-\mu_s z)]}{1+\frac{w_S^2}{w_H^2}} + [1-\exp(-\mu_s z)]^2\frac{w_H^2}{w_S^2}\right] \tag{2}$$

$$N = \frac{\alpha^2 P_R P_S \sigma_b}{\pi w_H^2}, \quad \left(\frac{w_s}{w_H}\right)^2 = 1 + \left[\frac{2w_0}{\rho_0(z)}\right]^2, \quad \rho_0(z) = \sqrt{\frac{3}{\mu_s z}}\frac{\lambda}{\pi\theta_{rms}}\left[\frac{nf}{z}\right] \tag{3}$$

Before the introduction of the EHF model, the anisotropy factor g of the mesoporous TiO_2 scattering films have been calculated from the Mie scattering model [26], which can be written as $g = <\cos(\theta_{rms})>$ with values of 0.002, 0.102, 0.527, and 0.297 for diameters of 20, 150, 300, and 500 nm respectively. With the above relations, we incorporated the algorithm in Matlab to solve for the value of the scattering coefficient μ_s. In the fitting process, the scattering coefficient of mesoporous TiO_2 scatter film acts as a free-running parameter with fixed scattering angle θ_{rms}. Then the final running parameter of scattering coefficient can be further fitted by numerical fitting process based on the EHF model. In the fitting process, the correlation factor (ρ) between the experimental result and the fitted A-scan signal have been calculated to approach the optimal ρ (for good agreement, $\rho = 1$) under the convergence condition. After obtaining the optimal μ_s, the single- and multiple-scattering effects can be separately quantified and drawn as the function of depth (Fig. 5(b)) to further analyze the relatively contribution of these two scattering effects in depth.

3. Results and Discussion

3.1 SEM Top View of TiO_2 Beads Samples

In order to confirm the morphologies, the top-view SEM images of mesoporous TiO_2 beads with different diameters ranged from 20 to 500 nm have been observed at the same scale, shown in Fig. 2. At fixed solvent concentration of 13 wt%, the variation in the TiO_2 crystal structure shows the disorder arrangements with various degrees of aggregation and dispersion, and the bead density is 8040, 17, 2.19, to 0.47 beads/μm^3 for bead diameter of 20, 150, 300, and 500 nm respectively.

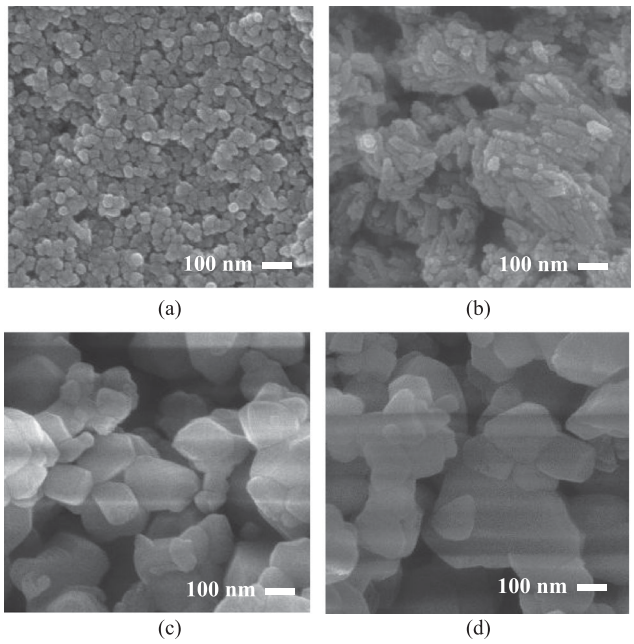

Fig. 2. SEM top-view sections of mesoporous TiO_2 beads with average diameter of (a) 20 nm; (b) 150 nm; (c) 300 nm; and (d) 500 nm.

In Fig. 2(a), the mesoporous TiO_2 beads with average diameter of 20 nm show the smallest inter-particle spacing between the TiO_2 beads, which form a closely packed structure with a flat surface. In Fig. 2(b), mesoporous TiO_2 beads show rod-like structure with the average diameter of 150 nm, accompanied with large amounts of aggregation. In both Fig. 2(c) and (d), average diameters of 300 and 500 nm, the mesoporous TiO_2 beads can be seen to form large irregular shapes. In comparison, under the same observation field, as the diameter of TiO_2 beads increases, the bead number decreases and the inter-particle spacing between adjacent beads increase. In addition, when the bead diameter is increased to 500 nm, the sample shows the largest inter-particle spacing and the smallest number of scattering particles.

3.2 Diffusive Reflectance Spectral Measurement

In Fig. 3, the normalized diffusive reflectance spectra of mesoporous TiO_2 films were measured in the wavelength range of 300∼1100 nm, as one of the methods commonly used to determine the optical scattering effects. The relative changes in the peak reflectance shows differences as the bead diameter varied, with R = 37% for 20 nm, R = 76% for 150 nm, R = 95% for 300 nm, and R = 90% for 500 nm. All samples show that the measured reflectivity peaks at wavelengths around 400 nm [11], [14], which is identified as a specific optical property of TiO_2 materials. According to the diffusive reflectance spectra, for smaller mesoporous TiO_2 beads (20 nm and 150 nm) the results are similar, with reflectivity peaks at the wavelengths around 409 nm. On the other hand, for the larger beads (300 nm and 500 nm), the reflectance peaks at wavelengths around 425 nm, which is a slight red-shift compared to the reflectance peaks for smaller TiO_2 beads due to the dominance of Mie scattering effect. In comparison, the mesoporous TiO_2 scattering film with bead diameter of 300 nm shows the highest reflectance intensity especially at the longer wavelengths. When increasing the bead diameter from 20 nm to 300 nm, the reflectance at the longer wavelength of 800 nm have been strongly enhanced from 43% to 70%, and a slight decreased to 67% for the bead diameter of 500 nm. Such strong reflectance enhancements (1.63 times) at the longer wavelengths are mainly contributed by the effect of multiple scattering [14].

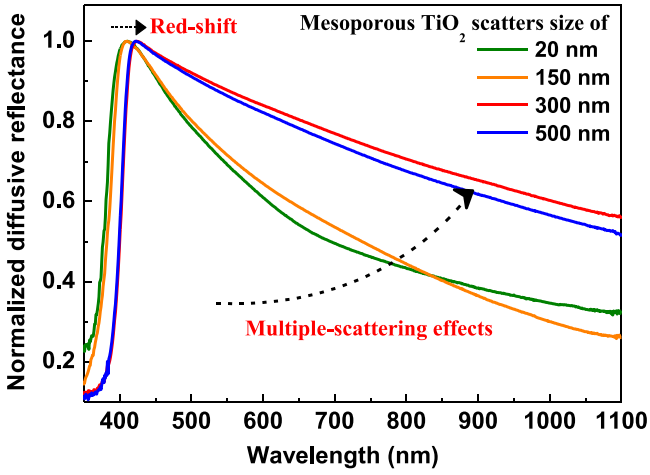

Fig. 3. Normalized diffusive reflectance spectra of mesoporous TiO_2 beads with the average bead diameters of 20 nm, 150 nm, 300 nm, and 500 nm, and measured for the wavelength ranged from 300 nm to 1100 nm.

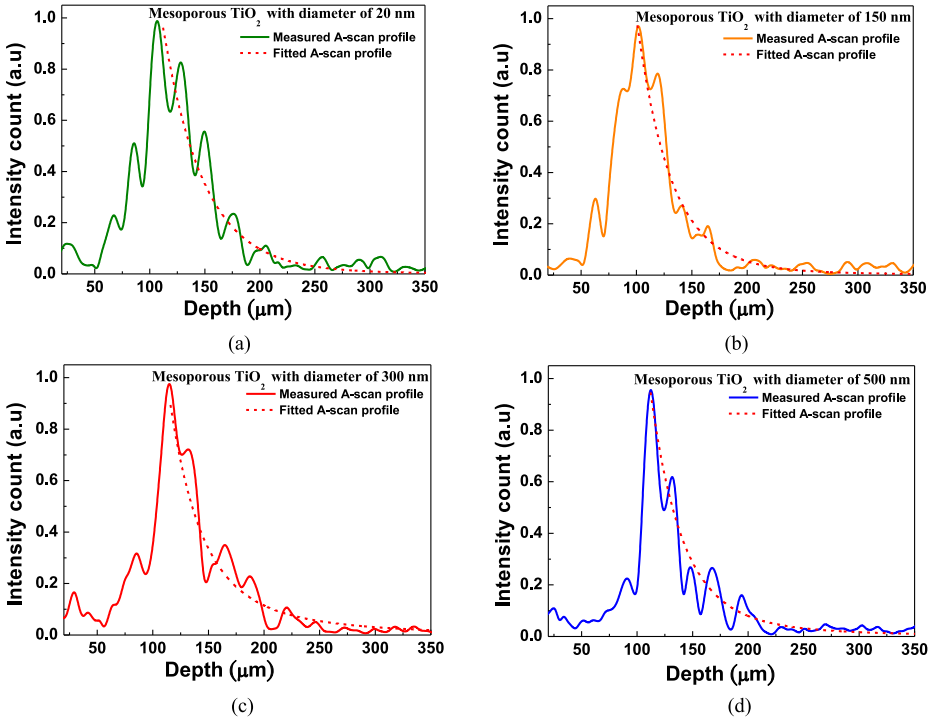

Fig. 4. Measured average A-scan profiles and fitted A-scan profiles of (a) Mesoporous TiO_2 film with average bead diameter of 20 nm and scattering coefficient of 13.5 ± 0.6 mm^{-1}. (b) Mesoporous TiO_2 film with average bead diameter of 150 nm and scattering coefficient of 16.5 ± 0.6 mm^{-1}. (c) Mesoporous TiO_2 film with average bead diameter of 300 nm and scattering coefficient of 20.2 ± 0.6 mm^{-1}. (d) Mesoporous TiO_2 film with average bead diameter of 500 nm and scattering coefficient of 18.5 ± 0.6 mm^{-1}.

3.3 Determination of Multiple Scattering Effects

In order to determine the size-dependent effect of single and multiple scattering at near-infrared wavelengths, the A-scan profiles extracted from the SD-OCT system is analyzed. In Fig. 4, both the measured (solid line) and fitted (dashed line) A-scan profiles are shown, and quite obviously the slopes of the individual curves are not equal. According to (1), the heterodyne factor $\psi(z)$ is modulated by the inhomogeneous optical properties of the samples, which consists of contribution

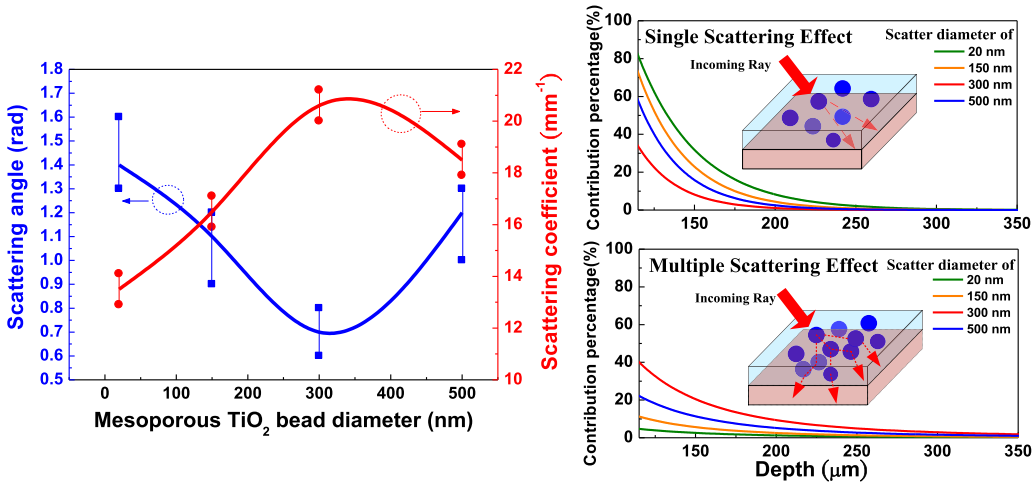

Fig. 5. (a). Fitted scattering coefficient (mm^{-1}) and scattering angle (rad) with various diameters of mesoporous TiO_2 beads based on extend Huygens-Fresnel model with the error bar, red line represents the scattering coefficient (right Y-axis) and blue line represents the scattering angle value (left Y-axis). (b) Contribution percentage of single- and multiple-scattering effects from TiO_2 beads for different diameters, and the inset schematic figures show the phenomenon of single- and Multiple-scattering effects.

from both the single and multiple scattering. With the Mie scattering model, the model is restricted to a single scattering of a spherical scattering particle, and for situations where large amounts of scattering and scattering particles are present, it is difficult to determine the scattering parameters, which is further compounded by the irregularities in the shapes of the scattering particles. In addition, multiple scattering occurs at the longer wavelength region. In the Mie scattering model, for a single spherical scattering particle with a single scattering, the scattering cross section can be described as C_{sca}, defined in (4). The scattering coefficient μ_s can be expressed as in (5),

$$C_{sca} = \frac{1}{I_0} \iint_{4\pi} I_{sca}(\theta) d\Omega. \tag{4}$$

$$\mu_s = C_{sca}/V. \tag{5}$$

where I_0 is the intensity of incident light, θ is the scattering angle (also correlated to the anisotropy factor $g = < \cos\theta >$), $I_{sca}(\theta)$ is the output scattering intensity depending on the scattering angle (θ), Ω is the integrated solid angle, and V is the volume of the scattering material. However in the OCT system, since the backscattered light from the sample is collected from the sample arm, the number of scatterings detected will be correlated to the finite area of sample arm probe. In this analysis method, we can obtain the results of single and multiple scattering effects at the near-infrared region. Furthermore, the dip/dump of signals can probably be attributed to the scattering effects with IPS between adjacent TiO_2 beads which can induce the similar interference pattern in space domain. In addition, the dip/dump of signals are hard to be expressed by EHF theory. Therefore, the optimal scattering coefficient of TiO_2 bead samples are fitted and obtained under the convergence condition by numerical fitting algorithm. Using (1), each curve was fitted with different values of the optical parameters to obtain the best-fitted results. In Fig. 5(a), the final scattering coefficient (μ_s) and effective scattering angle (θ_{rms}) are determined by the fitting algorithm, and the error bar represents the range of probable fitting values. For bead diameter of 20 nm, the smaller scattering coefficient of 13.5 ± 0.6 mm^{-1} is shown at the central wavelength of 853 nm, which is accompanied by a range of scattering angles from 1.3 to 1.6 rad. When increasing bead diameters to 150 nm, 300 nm, and 500 nm, the scattering coefficients are 16.5 ± 0.6 mm^{-1}, 20.2 ± 0.6 mm^{-1}, and 18.5 ± 0.6 mm^{-1}, respectively. The optimal μ_s of TiO_2 bead samples with different bead diameters

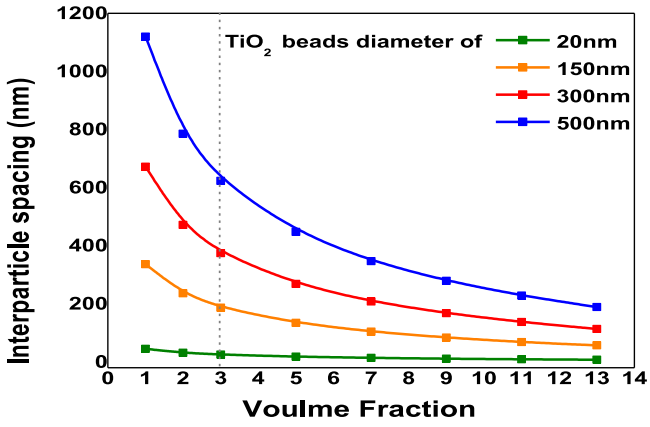

Fig. 6. The inter-particle distance against the different volume fraction of mesoporous TiO_2 beads with different diameters for 20 nm, 150 nm, 300 nm, 500 nm.

can be finally obtained with ρ of 0.94, 0.96, 0.97, 0.92 for the bead diameters of 20 nm, 150 nm, 300 nm, and 500 nm, respectively. On the other hand, with the Mie scattering model, the calculated effective scattering angles are 1.4, 1.1, 0.7, and 1.2 radians respectively.

After the fitting algorithm, the single and multiple scattering effects are quantified separately by extracting the optical parameters depending on the different sizes of the mesoporous TiO_2 beads in (1). In this study, we consider the relative contribution (%) of the scattering effects for the mesoporous TiO_2 samples. In Fig. 5(b), when increasing the bead diameters from 20 nm to 500 nm, the result shows a reduction of contribution from single scattering effect, from 80%, 71%, 33%, to 56% respectively, and a general increasing contribution from the multiple scattering effect, from 5%, 10%, to 40%, but then decreased to 22% respectively. According to the fitting results, we observe that the mesoporous TiO_2 at 300 nm have a significant contribution from the multiple scattering effects. Comparing with the diffusive reflectance spectra, the fitting results coincides with the enhancement of the multiple scattering effects at longer wavelengths for the mesoporous TiO_2 scatter diameter of 300 nm, due to the higher contribution of multiple scattering effects. Furthermore, the size dependent morphology of the mesoporous TiO_2 beads show the variations of optical characteristics, which consist of not only the Mie scattering effects based on single scattering, but also the multiple scattering effects dependent on the number of scattering particles.

3.4 Inter-Particle Distance With Volume Fraction of Mesoporous TiO_2 Beads Samples

In this study, we are going to emphasize the concept of inter-particle distance (IPS) between TiO_2 beads with different diameters embedded in the medium. Inter-particle distance can be defined as the distance from the surface of one scatter to that of another scatter. According to the reference [27], the IPS of TiO_2 beads suspension can be expressed as the function of volume faction in (6), where ϕ is the volume fraction, ϕ_m is maximum volume fraction, and r is the radius of TiO_2 beads, respectively. The volume fractions (ϕ) of TiO_2 samples with different diameters are fixed as 3%, and ϕ_m is 34%. As shown in Fig. 6, when increasing the diameters of TiO_2 beads from 20, 150, 300 to 500 nm, the IPS are increased from 25, 187, 373, to 623 nm, respectively. Comparing to the fitting result with EHF model in Fig. 5, we found that the contribution percentages of multiple scattering are increased from 5%, 10%, to 40%, and then decreased to 22% when IPS is increased from 25, 187, 373, to 623 nm, respectively. Therefore, within the short distance of 20 nm between scatters, the probability of re-directed light would be reduced if light scattered by the second or even more than two scatters. However, the condition for a larger IPS of 623 nm would result as independent TiO_2 beads to reduce the contribution percentage of multiple scattering effects, which is consistent with the results in Fig. 5. Therefore, from the Fig. 6, we can further consider the situation with higher concentration of scatters with a fixed diameter of TiO_2 bead and the larger volume fractions will be

accompanied with smaller IPS as can be expected. Similar results have also been observed in our measurement with the highest contribution percentage of single scattering effect at the smallest IPS. At the meantime, the single scattering effect enhanced would reduce the intensity reflected from the TiO_2 bead sample to make the scattering coefficient (μ_s) deviate from the predicted value based on Mie scattering model [21]. However, in this study, we only focus on the fixed volume fraction of TiO_2 beads with different diameters due to not only the difficulty in preparation of mesoporous TiO_2 sample with well dispersion in higher volume fraction, but also the result can be predicted without further experiments.

$$IPS = 2r\left(\left(\frac{\phi_m}{\phi}\right)^{1/3} - 1\right)(\phi \ll \phi_m) \tag{6}$$

As the results, quantifying the scattering light signal composed of single and multiple scattering can be achieved by measurements using the SD-OCT system, which are strongly affected by the geometric structure of mesoporous TiO_2 beads and the wavelength of light used, especially if large number of scattering particles are embedded in the scattering medium. In particular, in the near-infrared region, the multiple scattering effects are more significant as compared to short wavelengths. In recent years, such scattering films have gained popularity for many applications. For example, in enhancing light harvesting for photovoltaic devices, the scattering film would induce random scattering, which spreads the incident light, and increase the average path length a photon travels within the device. In such device, multiple scattering effects (light sub-diffusion) are more likely to occur with shorter mean free path, and the shortest mean free path of TiO_2 beads with 300 nm obtained could exploit the interaction effects between scattering events [28]. Therefore, in this study, we investigate not only the occurrence of near-infrared multiple scattering effects, but also experimentally quantified the size-dependent multiple scattering contribution ratios using the SD-OCT system. To our knowledge, this is the first time a SD-OCT system is used to experimentally distinguish the contribution ratio of infrared single and multiple scattering effects from mesoporous TiO_2 samples. The value of our work is to provide a new analysis method to further realize the appearance of multiple scattering effects at near-infrared region, supplying on various optical applications.

4. Conclusion

In this study, we successfully investigated the size-dependent multiple scattering effects of mesoporous TiO_2 samples using SD-OCT at near-infrared region, where the depth dependent A-scan profiles have been fitted based on the extend Huygens Fresnel model to quantify the contribution of both the single and multiple scattering effects. The mesoporous TiO_2 film with average bead diameter of 300 nm was shown to have the highest reflectivity at longer wavelength due to the larger contribution of the multiple scattering effects, verified by fitting results. In addition, this is the first time to utilize the SD-OCT system to analyze mesoporous TiO_2 beads with different average diameters to verify the existence of reflection enhancement at infrared region, and to quantify the multiple scattering effects contribution ratios to as a new analysis method to determine the multiple scattering effects.

Acknowledgment

The authors would like to thank Mr. Li-Jen Hsiao for the assistance on MATLAB software and Prof. Ching-Fuh Lin and Mr. Hung-Chang Hsu for the assistance of measurement instrument.

References

[1] B. Bill, N. Morris, M. Dubey, Q. Wang, and Q. H. Fan, "Electrophoretic deposited TiO_2 pigment-based back reflectors for thin film solar cells," *Opt. Exp.*, vol. 23, no. 3, pp. A71–A82, 2015.

[2] B. F. Huang, D. Chen, X. L. Zhang, R. A. Caruso, and Y.-B. Cheng, "Dual-function scattering layer of submicrometer-sized mesoporous TiO_2 beads for high-efficiency dye-sensitized solar cells," *Adv. Funct. Mater.*, vol. 23, no. 8, pp. 1301–1305, 2010.
[3] A. P. Popov, A. V. Priezzhev, J. Lademann, and R. Myllyla, "TiO2 nanoparticles as an effective UV-B radiation skin-protective compound in sunscreens," *J. Phys. D, Appl. Phys.*, vol. 38, no. 15, pp. 2564–2570, 2005.
[4] G. Veerappan *et al.*, "Multi-functionality of macroporous TiO2 spheres in dye-sensitized and hybrid heterojunction solar cells," *Langmuir*, vol. 30, no. 11, pp. 3010–3018, 2014.
[5] S. Hore, C. Vetter, R. Kern, H. Smit, and A. Hinsch, "Influence of scattering layers on efficiency of dye-sensitized solar cells," *Sol. Energy Mater. Sol. Cells.*, vol. 90, no. 9, pp. 1176–1188, 2006.
[6] W. Peng and L. Han, "Hexagonal TiO_2 microplates with superior light scattering for dye-sensitized solar cells," *J. Mater. Chem.*, vol. 22, pp. 20773–20777, 2012.
[7] S. Hore, P. Nitz, C. Vetter, C. Prahl, M. Niggemann, and R. Kern, "Scattering spherical voids in nanocrystalline TiO_2—Enhancement of efficiency in dye-sensitized solar cells," *Chem. Commun.*, vol. 15, pp. 2011–2013, 2005.
[8] H.-J. Koo, J. Park, B. Yoo, K. Yoo, K. Kim, and N.-G. Park, "Size-dependent scattering efficiency in dye-sensitized solar cell," *Inorg. Chim. Acta*, vol. 361, no. 3, pp. 677–683, 2008.
[9] C. F. Bohren and D. R. Huffman, *Absorption and Scattering of Light by Small Particles*. New York, NY, USA: Wiley, 1983.
[10] H. C. van de Hulst, *Light Scattering by Small Particles*. New York, NY, USA: Wiley, 1957.
[11] I. G. Yu, Y. J. Kim, H. J. Kim, C. Lee, and W. I. Lee, "Size-dependent light-scattering effects of nanoporous TiO2 spheres in dye-sensitized solar cells," *J. Mater. Chem.*, vol. 21, pp. 532–538, 2011.
[12] J.-C. Auger, V. A. Martinez, and B. Stout, "Theoretical study of the scattering efficiency of rutile titanium dioxide pigments as a function of their spatial dispersion," *J. Coat. Technol. Res.*, vol. 6, no. 1, pp. 89–97, 2009.
[13] L. E. Mcneil, A. R. Hanuska, and R. H. French, "Orientation dependence in near-field scattering from TiO_2 particles," *Appl. Opt.*, vol. 40, no. 20, pp. 3727–3736, 2001.
[14] L. E. Mcneil and R. H. French, "Multiple scattering from rutile TiO2 particles," *Acta Mater.*, vol. 48, nos. 18/19, pp. 4571–4576, 2000.
[15] D. Huang *et al.*, "Optical coherence tomography," *Science.*, vol. 254, no. 5033, pp. 1178–1181, 1991.
[16] Y. P. de León, J. L. Pichardo-Molina, and N. A. Ochoa, "Growth kinetics of concave nanocubes studied by optical coherence tomography," *Plasmonics*, vol. 9, no. 4, pp. 907–915, 2014.
[17] J. C. Y. Kah, T. H. Chow, B. K. Ng, S. G. Razul, M. Olivo, and C. J. R. Sheppard, "Concentration dependence of gold nanoshells on the enhancement of optical coherence tomography images: a quantitative study," *Appl. Opt.*, vol. 48, no. 1, pp. D96–D108, 2009.
[18] R. Grombe, L. Kirsten, M. Mehner, T. P.J. Linsinger, H. Emons, and E. Koch, "Feasibility of non-invasive detection of engineered nanoparticles in food mimicking matrices by Optical Coherence Tomography," *Food Chem.*, vol. 153, pp. 444–449, 2014.
[19] L. P. Zhou *et al.*, "Influence of different sized nanoparticles combined with ultrasound on the optical properties of in vitro normal and cancerous human lung tissue studied with OCT and diffuse reflectance spectra," *Laser Phys.*, vol. 24, no. 11, pp. 115606–115615, 2014.
[20] D. Levitz, L. Thrane, M. H. Frosz, and P. E. Andersen, "Determination of optical scattering properties of highly-scattering media in optical coherence tomography images," *Opt. Exp.*, vol. 12, no. 2, pp. 249–847259, 2004.
[21] L. Thrane, H. T. Yura, and P. E. Andersen, "Analysis of optical coherence tomography systems based on the extended Huygens–Fresnel principle," *J. Opt. Soc. Amer. A.*, vol. 17, no. 3, pp. 484–490, 2000.
[22] V. D. Nguyen, D. J. Faber, E. van der Pol, T. G. van Leeuwen, and J. K. Kalkman, "Dependent and multiple scattering in transmission and backscattering optical coherence tomography," *Opt. Exp.*, vol. 21, no. 24, pp. 29145–29156, 2013.
[23] B. Karamata, M. Laubscher, M. Leutenegger, S. Bourquin, and T. Lasser, "Multiple scattering in optical coherence tomography. I. Investigation and modeling," *J. Opt. Soc. Amer. A*, vol. 22, no. 7, pp. 1369–1378, 2005.
[24] A. Tycho, T. M. Joergensen, and L. Thrane, "Focusing problem in OCT: Comparison of Monte-Carlo simulations, the extended Huygens-Fresnel principle, and experiments," *Proc. SPIE*, vol. 3915, pp. 25–35, 2000.
[25] J. Fujimoto and W. Drexler, *Optical Coherence Tomography*. Berlin, Germany: Springer, 2008, pp. 73–115.
[26] S. A. Prahl, "Mie scattering calculators," 2006. [Online]. Available: http://omlc.ogi.edu/calc/mie_calc.html
[27] T. Hao and R. E. Riman, "Calculation of interparticle spacing in colloidal system," *J. Colloid Interface Sci.*, vol. 297, no. 1, pp. 374–377, 2006.
[28] M. Burresi, F. Pratesi, F. Riboli, and D. S. Wiersma, "Complex photonic structures for light harvesting," *Adv. Optical Mater.*, vol. 3, no. 6, pp. 722–743, 2015.